Rapid energy-level shifts in metals under intense inner-shell photoexcitation

Hikaru Kitamura

Department of Physics, Kyoto University, Sakyo-ku, Kyoto 606-8502, JAPAN

Abstract

Rapid energy-level shifts in metals due to intense near-edge photoexcitation of core electrons are investigated with the density-matrix formalism. Analytic theory indicates that, as the core-hole density increases, the core levels are lowered relative to the valence levels, leading to an enhancement of the band gap; its origin can be attributed to a large asymmetry between localized core and delocalized valence orbitals. The energy-level shifts are incorporated into the rate equation to compute time evolutions of near-edge photoabsorption spectra for metallic lithium irradiated by a vacuum ultraviolet laser pulse. Numerical results indicate saturable absorption due to a blue shift of the K-edge, leading to a nonlinear transmission of the laser pulse at high intensities.

Keywords: x-ray free-electron laser, inner-shell excitation, energy-level shift, saturable absorption

Email address: kitamura@scphys.kyoto-u.ac.jp (Hikaru Kitamura)

1. Introduction

The X-ray free-electron laser (XFEL) [1] has been gaining attention as a new, powerful light source to probe microscopic structures and ultrafast chemical processes in atoms, molecules, condensed matter and plasmas. The XFEL pulse can penetrate deeply into a material and induce resonant excitation of many inner-shell electrons to the valence band above the Fermi level [2, 3]. If the laser wavelength is sufficiently close to the inner-shell photoabsorption edge, it is possible to realize a cold solid with multiple core holes and extra valence electrons. In such a transient high-energy-density state, which may be called a *hollow-atom solid* [4], strong Coulomb field by multiple localized core holes can rapidly modify the electronic structure and optical constants, with possible applications to switching device [2]. The effects of energy-level shifts on photoabsorption spectra and Auger decay rates in multiple core-excited states would be crucial in many aspects of XFEL applications.

In this paper, we present a density-matrix theory to analyze electron-hole kinetics in simple metallic solids under intense inner-shell photoexcitation. We thus show that the core-valence band gap is transiently enhanced due to the strong electron-hole attraction in the localized core orbital. Numerical simulations indicate that a vacuum ultraviolet free-electron laser (VUV FEL) pulse passing through a metallic lithium target can induce a blue shift of the K-edge, leading to saturable absorption and nonlinear transmission when the intensity is sufficiently high.

2. Basic equations

For an initial cold material without a laser field, the energy level ϵ_k^σ and the orbital wave function $\psi_k^\sigma(\mathbf{r})$ for a one-electron state k with spin σ can generally be obtained through the unrestricted Hartree-Fock (UHF) method. When a laser field characterized by a time-dependent vector potential $\mathbf{A}(t)$ is applied, the Hamiltonian H may be expressed as [5]

$$H = \sum_{k\sigma} \epsilon_k^\sigma c_{k\sigma}^\dagger c_{k\sigma} - \sum_{k_1k_2k_3\sigma\sigma'} (V_{k_1k_2k_3k_3}^{\sigma\sigma'} - \delta_{\sigma\sigma'} V_{k_1k_3k_3k_2}^{\sigma\sigma}) \delta_{k_3\sigma'}^{\mathrm{occ}} c_{k_1\sigma}^\dagger c_{k_2\sigma}$$
$$+ \frac{1}{2} \sum_{k_1k_2k_3k_4\sigma\sigma'} V_{k_1k_2k_3k_4}^{\sigma\sigma'} c_{k_1\sigma}^\dagger c_{k_3\sigma'}^\dagger c_{k_4\sigma'} c_{k_2\sigma} + \frac{e}{m_\mathrm{e} c} \mathbf{A}(t) \cdot \sum_{k_1k_2\sigma} \mathbf{p}_{k_1k_2}^\sigma c_{k_1\sigma}^\dagger c_{k_2\sigma}, \tag{1}$$

where $c_{k\sigma}^\dagger$ and $c_{k\sigma}$ refer to the creation and annihilation operators, respectively, of an electron in the unperturbed state (k, σ). The matrix element of the electron momentum operator is given as $\mathbf{p}_{k_1k_2}^\sigma = \int d\mathbf{r} \psi_{k_1}^{\sigma *}(\mathbf{r}) (\hbar/i) \nabla \psi_{k_2}^\sigma(\mathbf{r})$, and

$$V_{k_1k_2k_3k_4}^{\sigma\sigma'} = \int d\mathbf{r}_1 \int d\mathbf{r}_2 \psi_{k_1}^{\sigma *}(\mathbf{r}_1) \psi_{k_2}^\sigma(\mathbf{r}_1) \frac{e^2}{|\mathbf{r}_1 - \mathbf{r}_2|} \psi_{k_3}^{\sigma' *}(\mathbf{r}_2) \psi_{k_4}^{\sigma'}(\mathbf{r}_2) \tag{2}$$

describes a Coulomb repulsion between the electrons. The quantity $\delta_{k\sigma}^{\mathrm{occ}}$ is defined as $\delta_{k\sigma}^{\mathrm{occ}} \equiv 1$ if state (k, σ) is occupied in the initial unperturbed state, and $\delta_{k\sigma}^{\mathrm{occ}} \equiv 0$ if unoccupied.

Kinetics of electrons may be analyzed on the basis of the microscopic Hamiltonian (1) through the quantum-statistical equation of motion for density matrices [5, 6],

$$i\hbar \frac{\partial}{\partial t} \langle \rho_{kk'\sigma} \rangle = \langle [\rho_{kk'\sigma}, H] \rangle \ . \tag{3}$$

Here, the one-electron density matrix $\langle \rho_{kk'\sigma} \rangle$ is defined as an expectation value of the electron-hole excitation operator $\rho_{kk'\sigma} \equiv c_{k\sigma}^\dagger c_{k'\sigma}$. The diagonal

part of the density matrix, $f_{k\sigma} \equiv \langle \rho_{kk\sigma} \rangle$, represents the population of state (k, σ).

In Eq (1), the ion motion and the scattering of photons are neglected; Eq. (1) is otherwise formally exact because the electron collision beyond the UHF approximation is taken into account through the third term on the right-hand side. Substitution of this term into Eq. (3), however, yields a two-electron density matrix $K^{\sigma\sigma_1}_{kk_3k_1k_2} \equiv \langle c^\dagger_{k\sigma} c^\dagger_{k_1\sigma_1} c_{k_2\sigma_1} c_{k_3\sigma} \rangle$, which in turn depends on the three-electron density matrix, and so on [7]. The resultant infinite hierarchy of correlation, accounting for the electron-hole many-body effects, is relevant to an assessment of core-hole screening, photoabsorption near-edge spectra, Auger decay rates, and so on. In this work, we make a simplification by adopting the Born approximation to the electron collision term.

3. Energy-level shifts

3.1. General formalism

The shift of energy levels due to electron excitation may be analyzed through the off-diagonal ($k \neq k'$) part of Eq. (3), which reads [5, 8]

$$\begin{aligned} i\hbar \frac{\partial \langle \rho_{kk'\sigma} \rangle}{\partial t} = (\epsilon^\sigma_{k'} - \epsilon^\sigma_k) \langle \rho_{kk'\sigma} \rangle \\ + \sum_{k_3} \Big[\Big(\tilde{\epsilon}^{\rm UHF}_{k'k_3\sigma} + \frac{e}{m_{\rm e}c} \mathbf{A}(t) \cdot \mathbf{p}^\sigma_{k'k_3} \Big) \langle \rho_{kk_3\sigma} \rangle \\ - \Big(\tilde{\epsilon}^{\rm UHF}_{k_3k\sigma} + \frac{e}{m_{\rm e}c} \mathbf{A}(t) \cdot \mathbf{p}^\sigma_{k_3k} \Big) \langle \rho_{k_3k'\sigma} \rangle \Big] \\ + i\hbar \frac{\partial \langle \rho_{kk'\sigma} \rangle}{\partial t} \Big]_{\rm coll} . \end{aligned} \tag{4}$$

The first term on the right-hand side proportional to $\langle \rho_{kk'\sigma} \rangle$ contains the unperturbed energy levels ϵ^σ_k and $\epsilon^\sigma_{k'}$; the shifts of these energies arise first

from the self-energy matrix in UHF, which is defined as

$$\tilde{\epsilon}^{\rm UHF}_{kk'\sigma} = \sum_{k_1k_2\sigma_1} (V^{\sigma\sigma_1}_{kk'k_1k_2} - \delta_{\sigma\sigma_1} V^{\sigma\sigma}_{kk_2k_1k'})[\langle\rho_{k_1k_2\sigma_1}\rangle - \delta_{k_1k_2}\delta^{\rm occ}_{k_1\sigma_1}] \ . \tag{5}$$

The electron collision term in Eq. (4) is defined as

$$\frac{\partial\langle\rho_{kk'\sigma}\rangle}{\partial t}\Big]_{\rm coll} = \frac{-i}{\hbar}\sum_{k_1k_2k_3\sigma_1} (V^{\sigma\sigma_1}_{k'k_3k_1k_2}\delta K^{\sigma\sigma_1}_{kk_3k_1k_2} - V^{\sigma\sigma_1}_{k_3kk_2k_1}\delta K^{\sigma\sigma_1}_{k_3k'k_2k_1}) \ , \tag{6}$$

where $\delta K^{\sigma\sigma_1}_{kk_3k_1k_2} \equiv K^{\sigma\sigma_1}_{kk_3k_1k_2} - \langle\rho_{kk_3\sigma}\rangle\langle\rho_{k_1k_2\sigma_1}\rangle + \delta_{\sigma\sigma_1}\langle\rho_{k_1k_3\sigma}\rangle\langle\rho_{kk_2\sigma}\rangle$ represents the correlation contribution to the two-electron density matrix. The energy-level shift stemming from the collision term can be obtained by solving an equation of motion analogous to Eq. (3) for $\delta K^{\sigma\sigma_1}_{kk_3k_1k_2}$ in the Born approximation, and retaining a term proportional to $\langle\rho_{kk'\sigma}\rangle$. We thus obtain [7, 8]

$$\begin{aligned}\frac{\partial\langle\rho_{kk'\sigma}\rangle}{\partial t}\Big]_{\rm coll} \approx \frac{i}{\hbar}\sum_{k_1k_2k_3\sigma_1}\Big(&\wp\frac{|V^{\sigma\sigma_1}_{k'k_3k_1k_2}|^2}{\epsilon^{\sigma}_{k_3}+\epsilon^{\sigma_1}_{k_2}-\epsilon^{\sigma_1}_{k_1}-\epsilon^{\sigma}_{k}} - \wp\frac{|V^{\sigma\sigma_1}_{kk_3k_1k_2}|^2}{\epsilon^{\sigma}_{k_3}+\epsilon^{\sigma_1}_{k_2}-\epsilon^{\sigma_1}_{k_1}-\epsilon^{\sigma}_{k'}}\Big) \\ &\times[f_{k_1\sigma_1}(1-f_{k_2\sigma_1}) + (f_{k_2\sigma_1}-f_{k_1\sigma_1})f_{k_3\sigma}]\langle\rho_{kk'\sigma}\rangle - \Gamma\langle\rho_{kk'\sigma}\rangle,\end{aligned} \tag{7}$$

where $\wp$ stands for the principal value. The damping factor $-\Gamma\langle\rho_{kk'\sigma}\rangle$, which gives rise to energy-level broadening [5], will be neglected in this section so far as the energy-level shift is concerned.

In Eq. (7), we may set $\epsilon^{\sigma}_{k_3} - \epsilon^{\sigma}_{k} \approx \epsilon^{\sigma}_{k'} - \epsilon^{\sigma}_{k_3} \approx 0$ (static-screening approximation [9]). Substitution of Eq. (7) into Eq. (4) then yields an energy-level shift for state (k,σ),

$$\Delta\epsilon_{k\sigma} = \tilde{\epsilon}^{\rm UHF}_{kk\sigma} + \tilde{\epsilon}^{\rm sc}_{k\sigma}, \tag{8}$$

with

$$\tilde{\epsilon}^{\rm sc}_{k\sigma} = -\sum_{k_1k_2k_3\sigma_1(k_1\neq k_2)} |V^{\sigma\sigma_1}_{kk_3k_1k_2}|^2 \frac{f_{k_2\sigma_1}-f_{k_1\sigma_1}}{\epsilon^{\sigma_1}_{k_2}-\epsilon^{\sigma_1}_{k_1}}(f_{k_3\sigma}-\delta^{\rm occ}_{k_3\sigma}) \tag{9}$$

denoting the electron screening within the Born approximation. Equation (8) provides an energy-level shift as a function of populations.

3.2. Application to simple metals

Let us apply formula (8) specifically to the core-valence excitation in alkali metals with initial energy gap $\epsilon_{\rm g}$ [8]. The wavefunction for the core band is approximated by a localized atomic core orbital, $\phi_{\rm c}(\mathbf{r}-\mathbf{R}_k)$, where $\mathbf{R}_k$ denotes the position of kth nucleus; the unperturbed core-orbital energy may be chosen as $\epsilon_k^\sigma = 0$ independent of k, assuming a completely flat band. For the valence band, we adopt a plane wave $\psi_{\mathbf{k}}^\sigma = \Omega^{-1/2} e^{i\mathbf{k}\cdot\mathbf{r}}$, with Ω being the volume of the system, and the free-electron-like energy dispersion, $\epsilon_{\mathbf{k}}^\sigma = \epsilon_{\rm g} + \hbar^2|\mathbf{k}|^2/2m_{\rm v}$, with $m_{\rm v}$ denoting the effective mass. The core-valence exchange is neglected.

Initially, the valence electrons occupy the states $|\mathbf{k}| \le k_{\rm F}$, where $k_{\rm F}$ denotes the Fermi wavenumber. Hence, the excited core electrons may enter the unoccupied states $k_{\rm F} < |\mathbf{k}| \le 2^{1/3}k_{\rm F}$ in the valence band. By assuming that all the core electrons have the same probability of excitation, we introduce a fraction $f_{\rm exc}$ of excited core electrons; the lowest valence band is fully occupied when $f_{\rm exc} = 0.5$. The shifts of core and valence energy bands, respectively, can then be expressed in terms of $f_{\rm exc}$ as [8]

$$\Delta\epsilon_{\rm c} = -2f_{\rm exc}\Big(\frac{U}{2} - \alpha_{\rm M}\frac{e^2}{a}\Big) + \frac{f_{\rm exc}}{\Omega}\sum_{\mathbf{q}} |F_{\rm c}(\mathbf{q})|^2 v(\mathbf{q})\Big[\frac{1}{\epsilon^{\rm v}(\mathbf{q})} - 1\Big]\,, \tag{10a}$$

$$\Delta\epsilon_{\mathbf{k}\rm v} = -\frac{2f_{\rm exc}}{\Omega}\sum_{\mathbf{q}(k_{\rm F}<|\mathbf{q}|\le 2^{1/3}k_{\rm F})} \frac{v(\mathbf{k}-\mathbf{q})}{\epsilon^{\rm v}(\mathbf{k}-\mathbf{q})}. \tag{10b}$$

Here, $U \equiv \int d\mathbf{r}_1 \int d\mathbf{r}_2 |\phi_{\rm c}(\mathbf{r}_1)|^2 |\phi_{\rm c}(\mathbf{r}_2)|^2 e^2/|\mathbf{r}_1-\mathbf{r}_2|$ refers to the on-site electron repulsion in the core orbital, $F_{\rm c}(\mathbf{k}) \equiv \int d\mathbf{r} |\phi_{\rm c}(\mathbf{r})|^2 e^{-i\mathbf{k}\cdot\mathbf{r}}$ denotes the core-electron form factor, $\alpha_{\rm M}$ refers to the Madelung constant of the lattice [10], and $a = (3/4\pi n_{\rm atom})^{1/3}$ with $n_{\rm atom}$ denoting the atomic number density;

$\epsilon^{\rm v}(\mathbf{q})$ is the dielectric function of the valence electrons [11] originating from Eq. (9). Here, strong electron correlation beyond the Born approximation is incorporated into $\epsilon^{\rm v}(\mathbf{q})$ through the local-field correction [11].

It turns out from Eqs. (10) that both the core and the valence bands are lowered ($\Delta\epsilon_{\rm c} < 0, \Delta\epsilon_{\mathbf{kv}} < 0$) as $f_{\rm exc}$ increases. The largest contribution arises from the first term on the right-hand side of Eq. (10a): The electrostatic interaction between an electron and a hole in the same core orbital amounts to $-U/2$ per electron, whereas the interaction between a core electron and an excited electron in the valence band amounts to $\alpha_{\rm M}e^2/a$ since the valence-electron distribution is spatially uniform. Because of the large asymmetry between the localized core and delocalized valence wavefunctions, $U/2 \gg \alpha_{\rm M}e^2/a$ holds; the core band is lowered more drastically than the valence band as $f_{\rm exc}$ increases, leading to an enhancement of the band gap, $\Delta\epsilon_{\rm g} \equiv \Delta\epsilon_{\mathbf{k}=0,{\rm v}} - \Delta\epsilon_{\rm c} > 0$.

A numerical example for K-shell excited metallic lithium [8] is presented in Fig. 1, where we have adopted $\alpha_{\rm M} = 1.79$ [body-centered-cubic (bcc) lattice], $n_{\rm atom} = 4.75 \times 10^{22}$ cm^{-3}, and $m_{\rm v} = 1.53m_{\rm e}$; $\phi_{\rm c}(\mathbf{r})$ has been approximated by a Slater-type 1s orbital with an exponent of 2.69. A large band-gap enhancement is clearly indicated as a result of the core-level lowering. As $f_{\rm exc}$ increases, however, careful attention should be paid to the treatment of valence-electron redistribution after a sudden appearance of core holes [12, 13]. It remains to be seen how a strong electron-hole correlation beyond the Born approximation influences the redistribution process and the resultant band gap of a real metal.

4. Saturable absorption

4.1. Rate equation

In Sec. 3, we have analyzed a relation between the energy-level shifts and populations. In this section, we derive a rate equation to simulate time evolutions of populations, energy-level shifts, and photoabsorption spectra in the presence of a laser pulse [5].

The population change is governed by the diagonal part of Eq. (3),

$$\frac{\partial f_{k\sigma}}{\partial t} = \frac{2}{\hbar} \sum_{k'(\neq k)} \mathrm{Im}\Big\{ \Big[\tilde{\epsilon}^{(0)}_{kk'\sigma} + \frac{e}{m_{\mathrm{e}}c} \mathbf{A}(t) \cdot \mathbf{p}^{\sigma}_{kk'} \Big] \langle \rho_{kk'\sigma} \rangle \Big\} + \Big[\frac{\partial \langle \rho_{kk\sigma} \rangle}{\partial t} \Big]_{\mathrm{coll}} , \quad (11)$$

with

$$\tilde{\epsilon}^{(0)}_{kk'\sigma} = \sum_{k_1 k_2 \sigma_1 (\neq k' k \sigma)} (V^{\sigma\sigma_1}_{kk'k_1k_2} - \delta_{\sigma\sigma_1} V^{\sigma\sigma}_{kk_2k_1k'}) [\langle \rho_{k_1k_2\sigma_1} \rangle - \delta_{k_1k_2} \delta^{\mathrm{occ}}_{k_1\sigma_1}] \, . \quad (12)$$

Instead of performing full numerical integrations of Eqs. (4) and (11), we solve the off-diagonal equation (4) within the Markov approximation [7]; the resultant solutions to $\langle \rho_{kk'\sigma}(t) \rangle$ at time t can be expressed in terms of the instantaneous values of the populations, $f_{k\sigma}(t)$ and $f_{k'\sigma}(t)$, ignoring their memory effects. Substitution of these solutions to Eq. (11) eliminates off-diagonal density matrices, yielding a rate equation describing time evolutions of collisional and radiative transitions [5]:

$$\frac{\partial f_{k\sigma}(t)}{\partial t} = \frac{I_\nu}{\hbar\omega_\nu} \sum_{k'(\neq k)} [\sigma^{\mathrm{abs}}_{kk'\sigma}(\omega_\nu) + \sigma^{\mathrm{emi}}_{kk'\sigma}(\omega_\nu)][f_{k'\sigma}(t) - f_{k\sigma}(t)] + \frac{1 - f_{k\sigma}(t)}{\tau^{\mathrm{in}}(k\sigma)} - \frac{f_{k\sigma}(t)}{\tau^{\mathrm{out}}(k\sigma)} \, . \quad (13)$$

Hereafter, we assume a linearly polarized monochromatic laser field, $\mathbf{A}(t) = \mathrm{Re}[\mathbf{A}_0 e^{-i\omega_\nu t}]$, with frequency ω_ν and intensity $I_\nu = \omega_\nu^2 |\mathbf{A}_0|^2 / 8\pi c$.

While the usual collisional-radiative rate equations for plasmas [14] are constituted by a set of transition probability data for individual atoms and ions, the rate coefficients that enter Eq. (13) are derived automatically from the Hamiltonian (1) incorporating time-dependent energy-level shifts. The photoabsorption cross-section accompanying an electron transition $k' \to k$, averaged over the directions of polarization, is given by

$$\sigma^{\rm abs}_{kk'\sigma}(\omega) = \frac{4\pi e^2}{c\hbar m_{\rm e}^2\omega}\frac{|\tilde{\mathbf{p}}^{\sigma}_{kk'}(\omega)|^2}{3}\frac{\Gamma}{[\omega-\tilde{\omega}^{\rm IVO}_{kk'\sigma}(t)]^2+\Gamma^2}\ , \tag{14}$$

where the renormalized transition frequency is expressed as

$$\hbar\tilde{\omega}^{\rm IVO}_{kk'\sigma}(t) \equiv \epsilon^{\sigma}_{k}-\epsilon^{\sigma}_{k'}+\Delta\epsilon_{k\sigma}(t)-\Delta\epsilon_{k'\sigma}(t)-(V^{\sigma\sigma}_{k'k'kk}-V^{\sigma\sigma}_{k'kkk'})[f_{k'\sigma}(t)-f_{k\sigma}(t)]\ . \tag{15}$$

Here, the energy-level shift $\Delta\epsilon_{k\sigma}(t)$ is given by Eq. (8) and it depends on t through $f_{k\sigma}(t)$. The last term on the right-hand side accounts for a lowering of the final-state level due to the creation of a hole in the initial-state level, known as the improved virtual-orbital correction [15]. An expression analogous to Eq. (14) can be found for the emission cross-section $\sigma^{\rm emi}_{kk'\sigma}(\omega)$ [5].

It must also be noted in Eq. (14) that the strength of radiative transition is determined by the renormalized momentum operator, which takes into account shielding of the laser field due to electron polarization [5],

$$\tilde{\mathbf{p}}^{\sigma}_{kk'}(\omega) = \mathbf{p}^{\sigma}_{kk'}+\frac{1}{\hbar}\sum_{k_1k_2\sigma_1(\neq kk'\sigma)}(V^{\sigma\sigma_1}_{kk'k_2k_1}-\delta_{\sigma\sigma_1}V^{\sigma\sigma}_{kk_1k_2k'})\frac{\omega-\tilde{\omega}^{\rm IVO}_{k_1k_2\sigma_1}(t)-i\Gamma}{[\omega-\tilde{\omega}^{\rm IVO}_{k_1k_2\sigma_1}(t)]^2+\Gamma^2}$$
$$\times[f_{k_2\sigma_1}(t)-f_{k_1\sigma_1}(t)]\tilde{\mathbf{p}}^{\sigma_1}_{k_1k_2}(\omega). \tag{16}$$

This expression corresponds to the random-phase approximation with exchange [16], which is a consequence of our use of the UHF approximation.

Analogous expression including dynamic electron correlation was previously derived [13] through the time-dependent density-functional formalism. We stress here that Eq. (16) is time-dependent.

The factors $1/\tau^{\rm in}(k\sigma)$ and $1/\tau^{\rm out}(k\sigma)$ refer to the rates of electrons entering and escaping out of state $(k\sigma)$, respectively, through collisional processes such as Auger decay and intraband relaxation. These quantities can be expressed in the form of a Boltzmann collision term when $\partial\langle\rho_{kk\sigma}\rangle/\partial t]_{\rm coll}$ is treated in the Born approximation with exchange [5].

4.2. K-edge shift in lithium

The theory developed in section 4.1 is applied to K-shell excitation of metallic lithium by VUV FEL. To simulate local photoresponse of electrons in the bulk solid, we consider a cluster of 24 atoms arranged in the bcc configuration, with the nearest-neighbor distance fixed at the bulk equilibrium length, 5.7 a.u [5]. The energy levels of the cluster have been computed through the UHF method by adopting the NDDO (neglect of diatomic differential overlap) approximation and Slater-type orbital basis sets consisting of 1s, 2s and 2p functions [17]. The discrete energy levels so obtained have been superimposed by a continuous energy spectrum of free electrons in the positive energy region. The broadening parameter Γ has been chosen as $\hbar\Gamma = 0.3$ eV, which is regarded as a phenomenological parameter mimicking the interaction of the cluster with the surrounding medium.

The electron screening beyond UHF approximation has been treated in a simplified fashion by setting $\tilde{\epsilon}^{\rm sc}_{k\sigma} = 0$ in Eq. (8) and truncating the Coulomb interaction $e^2/|\mathbf{r}_1 - \mathbf{r}_2|$ in Eq. (2) at the Thomas-Fermi screening distance, which is comparable to the nearest-neighbor distance.

We have solved Eq. (13) numerically for a square laser pulse with $\hbar\omega_\nu =$ 60 eV which is constantly applied throughout the period $0 \leq t \leq 40$ fs. Though our previous paper [5] treated only the case of $I_\nu = 10^{14}$ W/cm^2, the present work presents more systematic calculations for various intensities. The photoabsorption coefficient at time t and photon frequency ω is evaluated in accordance with Eq. (14) as

$$\kappa_{\rm abs}(\omega) = \frac{n_{\rm atom}}{N} \sum_{kk'\sigma} \sigma^{\rm abs}_{kk'\sigma}(\omega)[f_{k'\sigma}(t) - f_{k\sigma}(t)] \ , \tag{17}$$

with $N(= 24)$ being the total number of atoms in the cluster. Numerical results are displayed in Fig. 2 for $t = 40$ fs. It can be observed that the position of the K-edge shifts to high-energy side and $\kappa_{\rm abs}(\omega_\nu)$ takes on significantly reduced values at high intensities.

We note in Fig. 2 that the calculated K-edge energy in the initial state turns out somewhat higher than the experimental value, 55 eV, due to Haensel et al [18]. The position of the K-edge is affected sensitively by the renormalization effect of the dipole transition matrix shown in Eq. (16). We also remark that the experimental absorption spectrum [18] exhibits a broad maximum at 64 eV, which cannot be reproduced by the present theory. This may imply that the orbitals higher than 3s should be added to the basis set for more accurate description of the spectrum above the K-edge.

Let us compare the K-edge shift in Fig. 2 and the band-gap shift in Fig. 1. From the rate-equation analysis, the fraction of excited core electrons turns out $f_{\rm exc} = 0.026$ and 0.126 for $I_\nu = 10^{13}$ and 10^{14} W/cm^2, respectively; the corresponding shift of the band gap predicted in Fig. 1 amounts to 0.78 eV and 3.6 eV, respectively. These values are roughly consistent with the

magnitude of the K-edge shift. We find in Fig. 2, however, that the spectrum does not exhibit a constant shift but the spectral shape also changes, as exposed by the broadening of the absorption peak. Such a complicated change in the spectral shape is related to the broadening of the core band width, which is neglected in the simplified analysis in Sec. 3. We note that the fraction of electrons ionized above vacuum level stays below 0.01 so that the system is electrically quasi-neutral.

Time evolutions of $\kappa_{\rm abs}(\omega_\nu)$ are plotted in Fig. 3, where the photon energy is $\hbar\omega_\nu = 60$ eV. For $I_\nu < 10^{12}$ W/cm^2, $\kappa_{\rm abs}(\omega_\nu)$ is virtually constant, whereas a significant reduction of $\kappa_{\rm abs}(\omega_\nu)$ is predicted for higher I_ν values, indicating a saturable absorption within a timescale of 10 fs. This timescale is shorter than the Auger lifetime of a core hole estimated from $1/\tau^{\rm in}(k\sigma)$, which amounts to about 200 fs. By treating electron redistribution effects through Green's function formalism and adopting spherical waves for Auger electrons, Almbladh et al. [19] estimated the Auger lifetime of a lithium metal to be 39 fs; this value is far smaller than the present estimation based on the Born approximation but still longer than the timescale of absorption saturation.

We also remark in Fig. 3 that $\kappa_{\rm abs}(\omega_\nu)$ does not decrease monotonically but exhibits a hump. We have found that the hump appears when a core electron localized at a particular atom is excited more efficiently than the other electrons; in such a case, some energy levels are lowered but others are elevated within the same core band, leading to a broadening of the core band width [5]. More detailed analysis of the core-hole dynamics is needed in future studies.

4.3. Nonlinear transmission

The numerical data indicated in Fig. 3 have been obtained by neglecting a spatial variation of the laser field; hence, they would be valid on a *mesoscopic* spatial scale comparable to the laser wavelength (21 nm in the present example). The transmission coefficient of a laser pulse through a *macroscopic* sample is evaluated as follows: The local intensity of the laser propagating toward z-direction may obey the relation [20],

$$\frac{\partial I(z,t)}{\partial z} = -\kappa_{\rm abs}(\omega_\nu, I(z,t))I(z,t) \ . \tag{18}$$

This equation is a generalization of the Lambert-Beer law to the case of saturable absorption, where $\kappa_{\rm abs}$ is a function of the local intensity $I(z,t)$.

For a fixed z, the t-dependence of $\kappa_{\rm abs}(\omega_\nu, I(z,t))$ can be extracted from the data in Fig. 3 through numerical interpolation. Spatial integration of Eq. (18) for a given t with an initial condition $I(0,t) = I_\nu$ yields a transient intensity profile $I(z,t)$. The profiles at $t = 40$ fs are displayed in Fig. 4. The curve for $I_\nu = 10^{12}$ W/cm^2 exhibits a usual exponential decay $I(z,t) \approx I(0,t)\exp[-\kappa_{\rm abs}(\omega_\nu)z]$, whereas enhanced penetration of the laser pulse can be seen at higher intensities due to saturation.

The transmission coefficient of the laser pulse can be computed as

$$T_{\rm trans} = \frac{1}{I_\nu \Delta t}\int_0^{\Delta t} dt I(L,t) \ , \tag{19}$$

where L and Δt denote the sample thickness and the laser pulse width, respectively. Figure 5 displays numerical results for $L = 200$ nm and $\Delta t = 40$ fs. The steep increase of $T_{\rm trans}$ can be clearly observed in the region $I_\nu \gtrsim 10^{13}$ W/cm^2, indicating a nonlinear transmission due to saturable absorption.

Here, the population inversion factor $f_{k'\sigma}(t) - f_{k\sigma}(t)$ in Eq. (17) plays a minor role in saturation, because the fraction of excited core electrons is as small as 0.126 even at the highest intensity; the origin of the saturable absorption is dominated rather by the decrease of $\sigma^{\rm abs}_{kk'\sigma}(\omega)$ due to K-edge shift.

Experimentally, nonlinear transmission of a VUV FEL pulse has been observed for N-shell excitation of Sn [2] and L-shell excitation of Al [3]; the former case exhibits a nonlinearity much stronger than that in Fig. 5, indicative of ultrafast switches. Direct simulations of those heavy metals are required.

5. Concluding remarks

In a neutral hollow-atom solid consisting of multiple core holes and extra valence electrons above the Fermi level, we have predicted an increment of the band gap due to the attractive electron-hole interaction in the localized core orbital. Such a band-gap enhancement can be achieved transiently while an intense VUV FEL pulse propagating through a metallic target induces a rapid near-threshold core-valence excitation. Numerical simulations for K-edge excitation of lithium indicates that the laser pulse causes a blue shift of the K-edge, which in turn reduces the attenuation of the laser pulse itself. This mechanism can account for a nonlinear increase of the transmission coefficient as a function of the laser intensity, which was observed for some metals by recent VUV FEL experiments.

The present theory has adopted the crude Born approximation for the electron collision term. Strong electron-hole correlation effects beyond the Born approximation have to be included in order to obtain more accurate

data. While the present simulation has been limited to VUV excitation of a light metal, its extension to deep core-electron excitation by XFEL is necessary.

Acknowledgments

The author wishes to thank Dr. G. Gregori, Dr. S.J. Rose and Dr. H. Yoneda for pertinent discussions. This work was supported in part by a Grant-in-Aid for Promotion of Utilization of X-Ray Free-Electron Lasers provided by the Ministry of Education, Culture, Sports, Science and Technology in Japan.

References

[1] P. Schmüser, M. Dohlus and J. Rossbach, *Ultraviolet and Soft X-Ray Free-Electron Lasers* (Springer, Berlin, 2008).

[2] H. Yoneda, Y. Inubushi, T. Tanaka, et al., Opt. Express **17**, 23443 (2009); Y. Inubushi, H. Yoneda, A. Higashiya, et al., Rev. Sci. Instrum. **81**, 036101 (2010).

[3] B. Nagler, U. Zastrau, R.R. Fäustlin, et al., Nature Phys. **5**, 693 (2009).

[4] H. Kitamura, Chem. Phys. Lett. **475**, 227 (2009).

[5] H. Kitamura, J. Phys. B: At. Mol. Opt. Phys. **43**, 115601 (2010).

[6] A. Yariv, *Quantum Electronics*, Third Edition (Wiley, 1989), Chap. 1.

[7] F. Rossi and T. Kuhn, Rev. Mod. Phys. **74**, 895 (2002).

[8] H. Kitamura, Europhys. Lett. **94**, 27005 (2011).

[9] H. Haug and S.W. Koch, *Quantum Theory of the Optical and Electronic Properties of Semiconductors* (World Scientific, Singapore, 2003), Chap. 9.

[10] L.L. Foldy, Phys. Rev. B **17**, 4889 (1978).

[11] S. Ichimaru, *Statistical Plasma Physics, Vol. 2 Condensed Plasmas* (Addison-Wesley, Reading, 1994), Chap. 3.

[12] K. Ohtaka and Y. Tanabe, Rev. Mod. Phys. **62**, 929 (1990).

[13] A.L. Ankudinov, A.I. Nesvizhskii and J.J. Rehr, Phys. Rev. B **67**, 115120 (2003).

[14] H.-K. Chung, W.L. Morgan and R.W. Lee, J. Quant. Spectrosc. Radiat. Transfer **81**, 107 (2003).

[15] W.J. Hunt and W.A. Goddard III, Chem. Phys. Lett. **3**, 414 (1969).

[16] M. Ya. Amusia, *Atomic Photoeffect* (Plenum, NY, 1990), Chap. 4.

[17] E. Clementi and C. Roetti, At. Data Nucl. Data Tables **14**, 177 (1974).

[18] R. Haensel, G. Keitel, B. Sonntag, C. Kunz and P. Schereiber, Phys. Stat. Sol. A **2**, 85 (1970).

[19] C.-O. Almbladh, A.L. Morales and G. Grossmann, Phys. Rev. B **39**, 3489 (1989).

[20] L. Allen and J.H. Eberly, *Optical Resonance and Two-Level Atoms* (Dover, NY, 1987), Sec. 6.5.

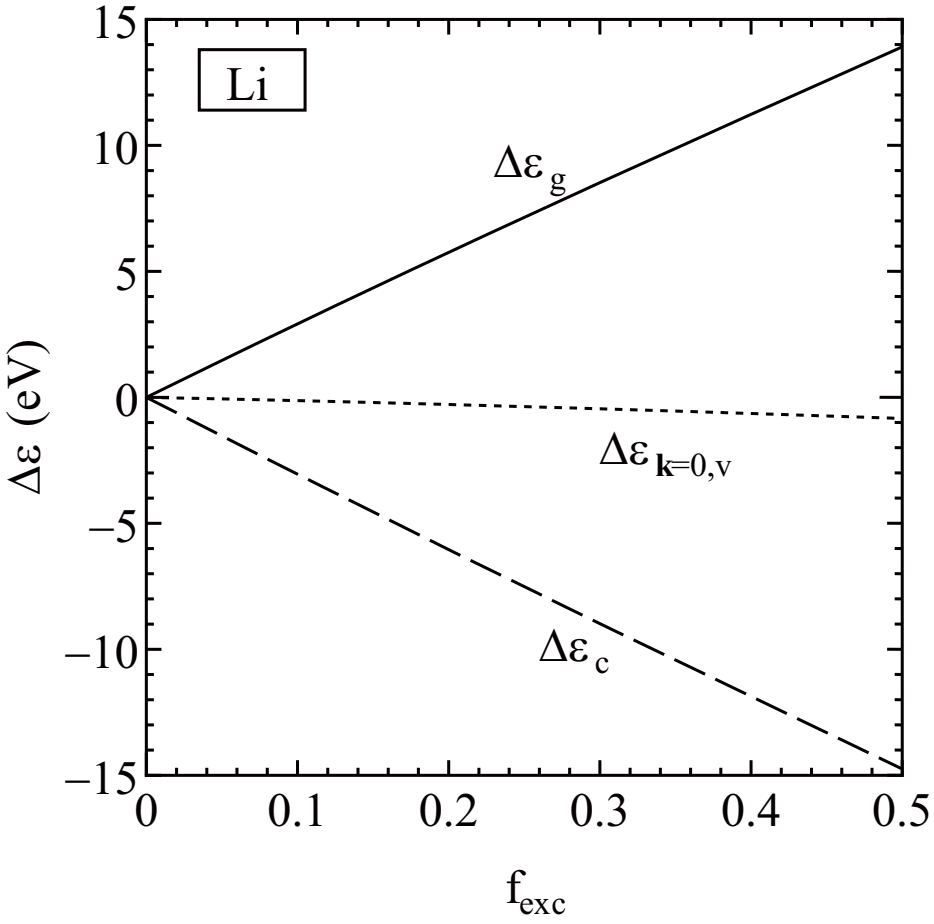

Figure 1: Energy-level shifts in lithium.

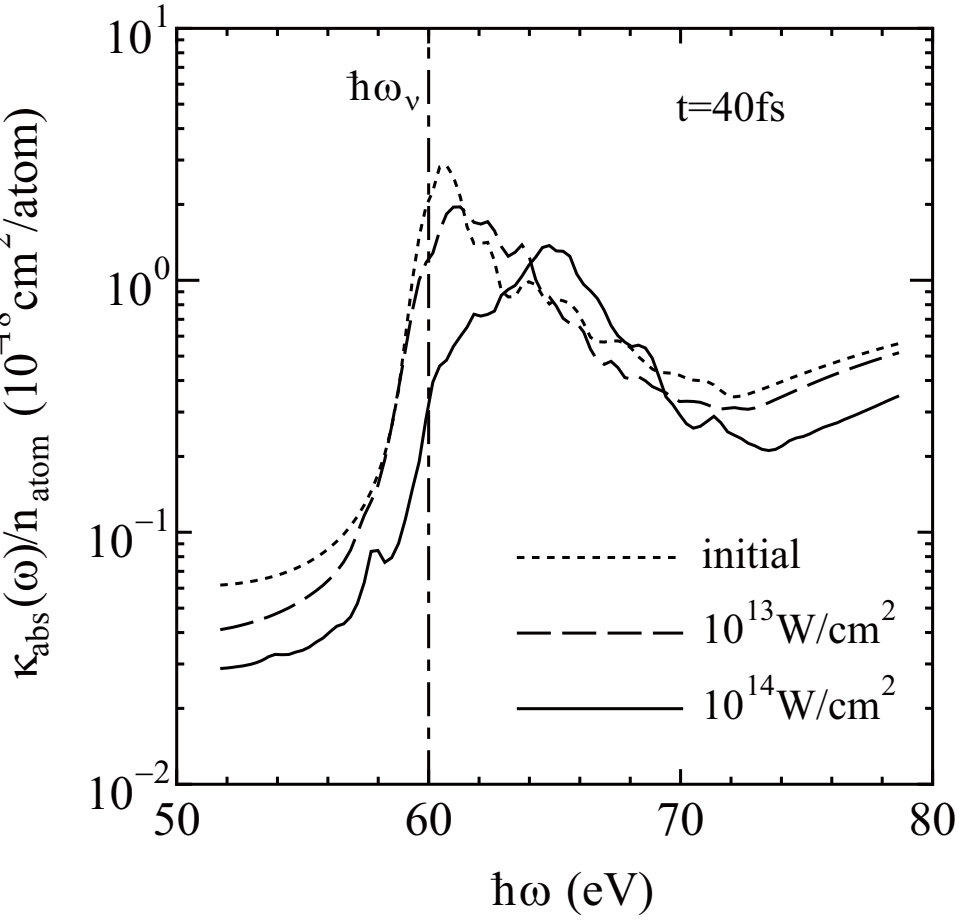

Figure 2: Photoabsorption spectra of lithium near the K-edge at $t = 40$ fs. The solid and the dashed curves represent the spectra for $I_\nu = 10^{14}$ W/cm^2 and 10^{13} W/cm^2, respectively. For comparison, the spectrum of the initial cold solid is indicated by the dotted curve.

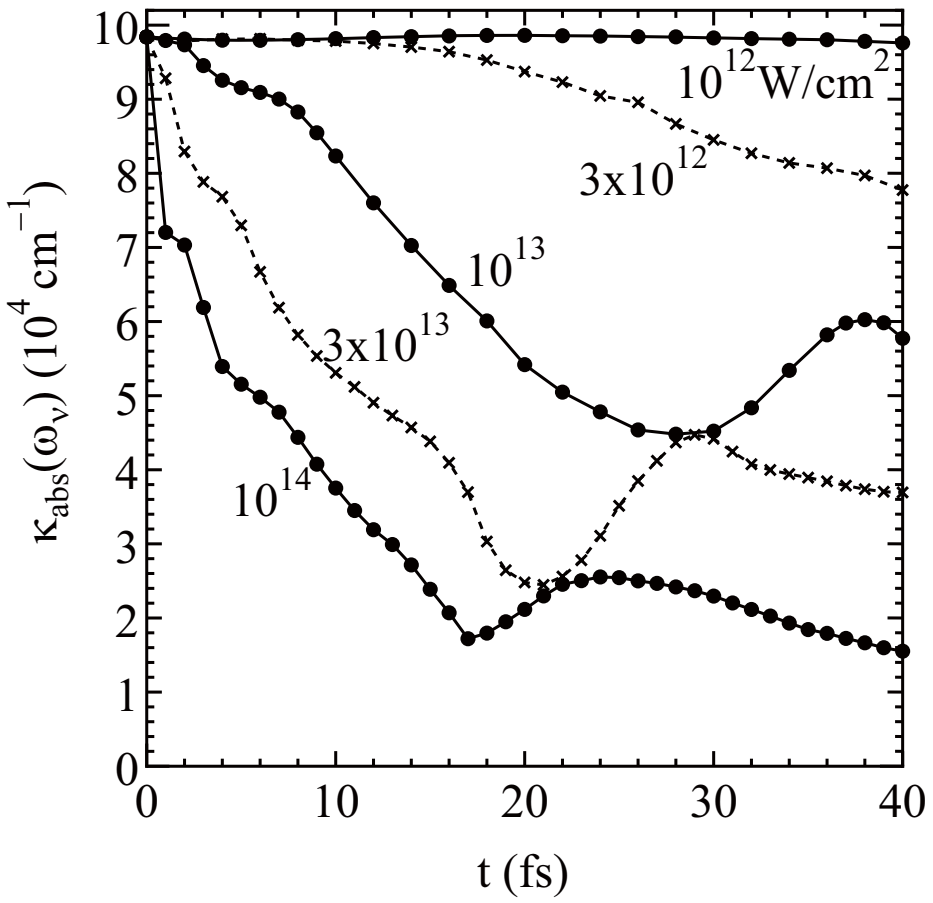

Figure 3: Time evolutions of the photoabsorption coefficients at $\hbar\omega = 60$ eV for various values of I_ν.

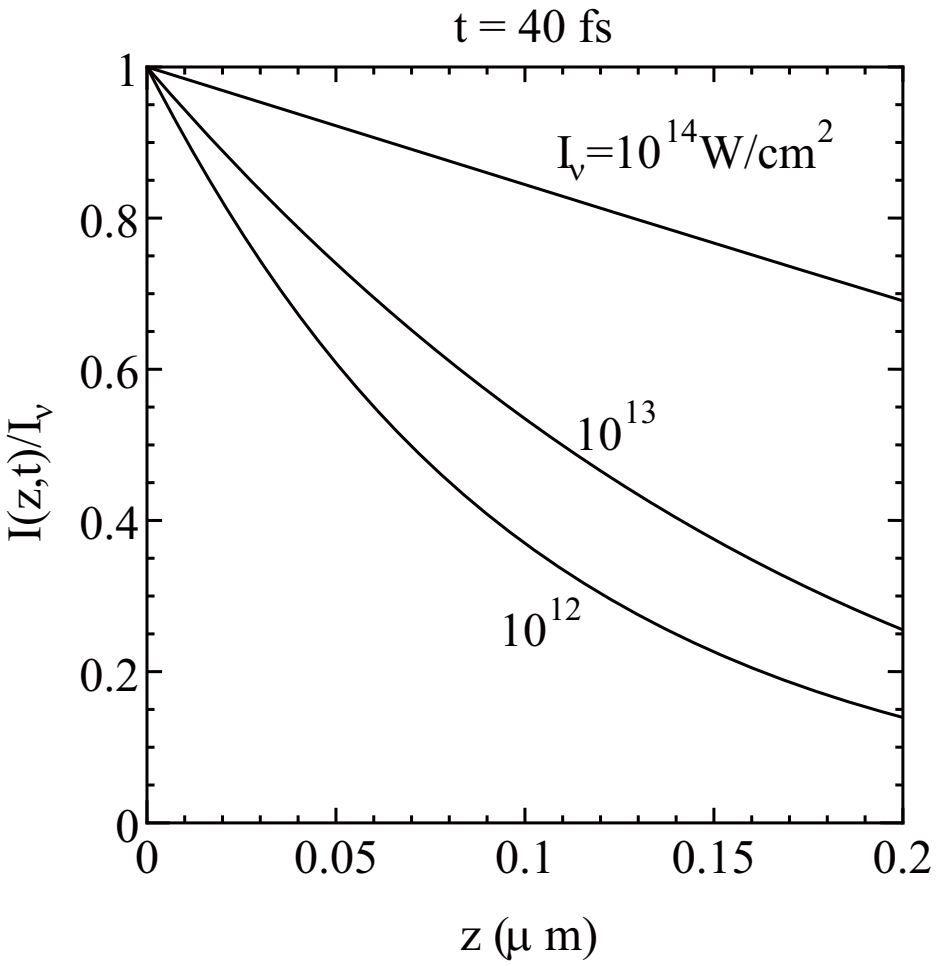

Figure 4: Attenuation of the laser pulse inside a lithium target measured at $t = 40$ fs.

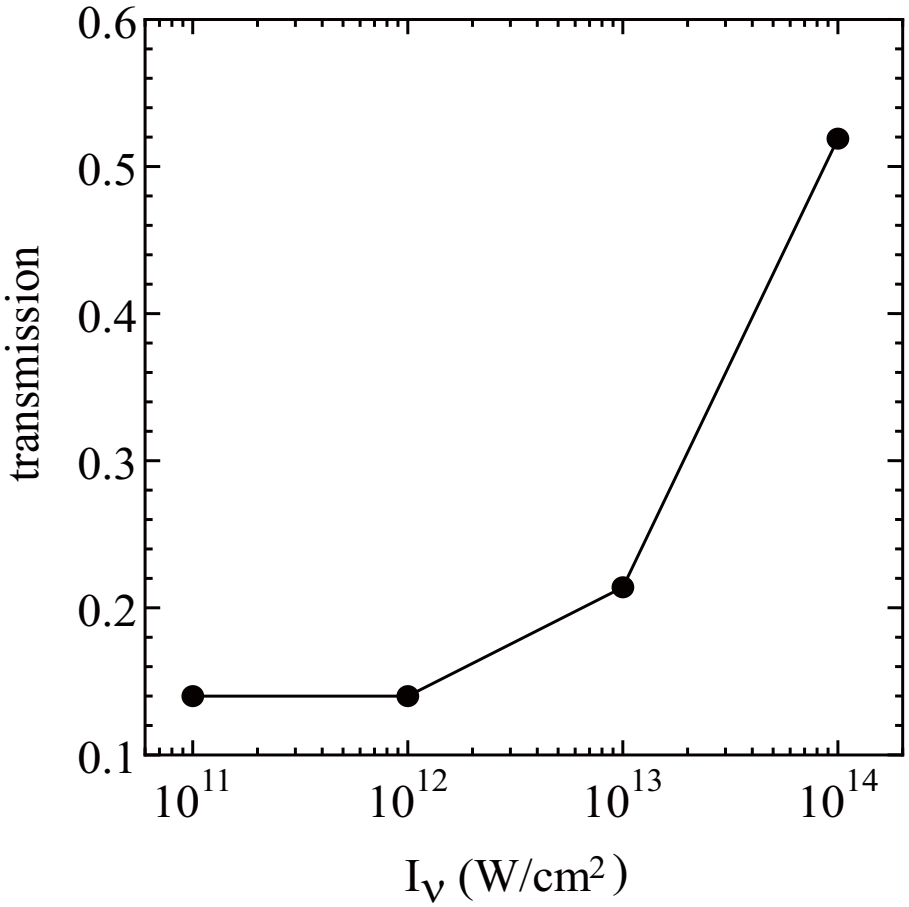

Figure 5: Transmission coefficient of the laser pulse through a lithium target.